Check for updates

A new swelling - creep model for red-bed mudstone and its application

Hongyi Yan[1], Feng Yu[2]*, Chaobo Zhu[2], Jianwei Yuan[2], Qiang Wang[2] and Jiang Wu[2]

[1]College of Civil and Construction Engineering, Hunan Institute of Technology, Hengyang, Hunan, China, [2]Sichuan Third Geological Brigade, Chengdu, Sichuan, China

In the red-bed region, engineering structures often encounter safety risks due to the swelling and creep properties of mudstone. Presently, there is a deficiency in constitutive equations capable of characterizing mudstone behavior under combined stress and swelling. To tackle this challenge, the deformation characteristics of red-bed mudstone were summarized based on the previous experimental data. A new element combination model (namely, swelling-creep model), comprising a Burgers body, swelling body, and nonlinear damper, was established to describe attenuated creep, swelling deformation, and accelerated creep, respectively. Based on this, the three-dimensional constitutive equations of the swelling-creep model were derived. Subsequently, based on the UDM program of FLAC^{3D}, the model was further developed using C++ language. Additionally, the developed swelling-creep model was validated through the numerical simulation experiments. Finally, the swelling-creep deformation process of red-bed mudstone under tensile stress conditions was simulated using the developed swelling-creep model. The research results indicate that the fitting results of the swelling-creep model are in good agreement with the experimental data, demonstrating its accuracy in describing the swelling and creep characteristics of red-bed mudstone. Moreover, when red-bed mudstone is subjected to axial tensile stress, the swelling effect significantly increases the axial strain rate and accelerates the transition to the accelerated creep stage.

KEYWORDS

red-bed mudstone, swelling-creep, constitutive model, numerical simulation, FLAC^{3D}

1 Introduction

Soft rock, notably mudstone and shale, represents a pervasive geological formation, encompassing roughly 50% of the Earth's surface (Hayano et al., 2001; Yu et al., 2017; Jia et al., 2021). Mudstone is characterized by its inherently low strength and pronounced rheological behavior (Lu et al., 2017; Chen et al., 2025). Furthermore, it exhibits a propensity to soften upon contact with water (Lu et al., 2017; Huang et al., 2023a) and undergo significant swelling (Doostmohammadi et al., 2009; Kong et al., 2018). The swelling-creep deformation, caused by changes in stress and moisture fields, plays a pivotal role in impacting the long-term stability of soft rock engineering (Hashiba and Fukui, 2016; Kong et al., 2018). The engineering cases revelated that the evolution of soft rock engineering activity, from initial deformation to ultimate

instability, entails a complex nonlinear gradual process (Yu et al., 2017; Liu et al., 2024). Hence, the development of a constitutive model capable of characterizing the coupled deformation process involving swelling and creep in mudstone holds paramount theoretical significance.

Since the 1950s, scholars have conducted extensive research on rock creep models, with many advancements in rock creep theory are grounded in the elemental model theory, particularly the composite creep element model composed of three fundamental linear elements: Hooke (H), Newtonian (N), and Saint Venant (S). While conceptually clear and structurally simple, this model falls short in capturing nonlinear phenomena such as accelerated creep (Zhang et al., 2004; Fan and Gao, 2007). Furthermore, existing constitutive models encounter substantial challenges in characterizing the influence of water environments on mudstone deformation. For instance, the swelling deformation process in mudstone is notably challenging to incorporate into these models, constituting one of the key hurdles that this study aims to address.

The swelling of mudstone is a long-term, complex process involving both physical and chemical interactions, influenced by water infiltration and stress release (Einstein, 1989; Steiner, 1993). According to Zhang et al. (2010), the swelling deformation of mudstone corresponds closely to its water absorption behavior, as demonstrated in their experiments. Under water immersion conditions, the swelling strain increases rapidly at first, then gradually transitions into a stable phase (Huang et al., 2023b; Huang et al., 2024). While the swelling deformation in typical swelling rocks typically proceeds swiftly, certain less resilient swelling mudstone exhibited noteworthy temporal effects (Madsen, 1999; Zhong et al., 2019). Therefore, owing to the time-dependent swelling characteristics of weaker swelling rock, accounting for water influence in the creep behavior of such rock is indispensable (Chen et al., 2023; Chen et al., 2024). Many scholars have considered water content in rock creep experiments and introduced water content or seepage as variable parameters into the creep equations through effective stress and variable substitution within damage mechanics. However, the entire hydration swelling process in rock involves a sequence of physical and chemical transformations, making it incomplete to solely address the impact of water content on rock creep. Hence, there is a compelling need to establish a model capable of describing the swelling-creep deformation process of rocks under the influence of both loading and water environments.

In this study, a novel swelling-creep model was developed to capture attenuated creep, swelling deformation, and accelerated creep. Three-dimensional constitutive equations for the model were derived, and it was implemented using C++ language within the UDM program of FLAC^{3D}. Validation was conducted through numerical simulations, and the model was then employed to simulate the swelling-creep deformation process of red-bed mudstone under tensile stress conditions.

2 Swelling-creep characteristics in red-bed mudstone

This study analyzes a swelling-creep coupled test, using the hydration-induced swelling-creep experiments on mudstone conducted by Zhang (2020) as a representative example. This experiment differs from traditional tests in that the hydration swelling of the rock sample and the applied stress load occur simultaneously (water is injected into the container immediately upon applying the load). This test is designed to capture the hydration swelling deformation characteristics of mudstone. As shown in Figure 1, the hydration swelling deformation characteristics of mudstone are correlated with the applied axial load. When the applied load is less than about 3 MPa, the mudstone exhibits a clear hydration swelling phase. However, when the load exceeds 4 MPa, the swelling deformation of mudstone cannot be observed.

The results indicate that the swelling deformation process of mudstone encompasses four key stages: attenuated creep, stable creep, accelerated creep, and swelling deformation. However, existing models fail to simultaneously capture all these deformation characteristics. Therefore, this study aims to develop a novel model that accurately represents the swelling-creep deformation behavior of red-bed mudstone.

3 Establishment of the swelling-creep model

In this study, a model that can describe the swelling and creep characteristics of red-bed mudstone will be established by serially connecting the Burgers model, swelling model, and nonlinear damper.

3.1 Burgers model

As shown in Figure 2, the Burgers model, consisting of a Maxwell body and a Kelvin body in series, can effectively describe the instantaneous deformation, attenuated creep, and stable creep of rock.

The one-dimensional strain equation of the Burgers model is presented in Equation 1:

$$\varepsilon = \frac{\sigma}{E_1} + \frac{\sigma}{\eta_1}t + \frac{\sigma}{E_2}\left[1 - \exp\left(-\frac{E_2}{\eta_2}t\right)\right] \tag{1}$$

where E_1, η_1 are the elastic modulus and viscosity coefficient of the Maxwell body, respectively; E_2, η_2 are the elastic modulus and viscosity coefficient of the Kelvin body, respectively.

3.2 Swelling model

The swelling deformation process of mudstone will be characterized by the swelling model (Sun, 1999). As shown in Figure 3, the model is primarily composed of a linear damper and a swelling element connected in parallel. Wherein, damper is used to depict the temporal characteristics of swelling deformation, while the swelling element is employed to characterize the stress-strain relationship during the mudstone swelling process (P represents the internal swelling force within the rock).

The one-dimensional constitutive equation of the swelling model is presented in Equation 2:

$$\eta\dot{\varepsilon} = \sigma + p(\varepsilon) \tag{2}$$

FIGURE 1
Swelling-creep strain curve of mudstone under **(a)** 1 MPa, **(b)** 2 MPa, **(c)** 3 MPa, **(d)** 4 MPa, **(e)** 5 MPa, **(f)** 6 MPa stress.

FIGURE 2
Burgers model.

FIGURE 3
Swelling model.
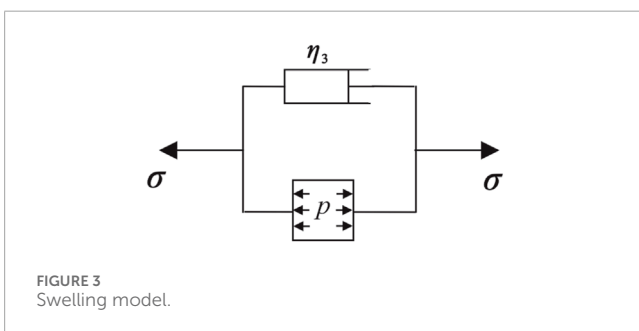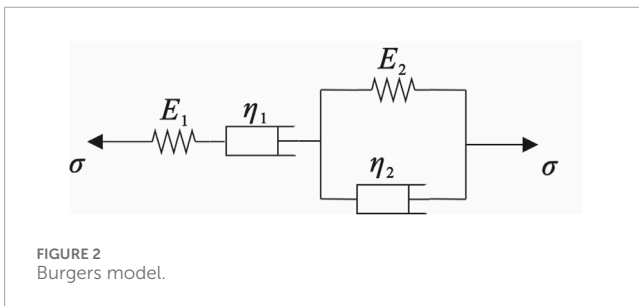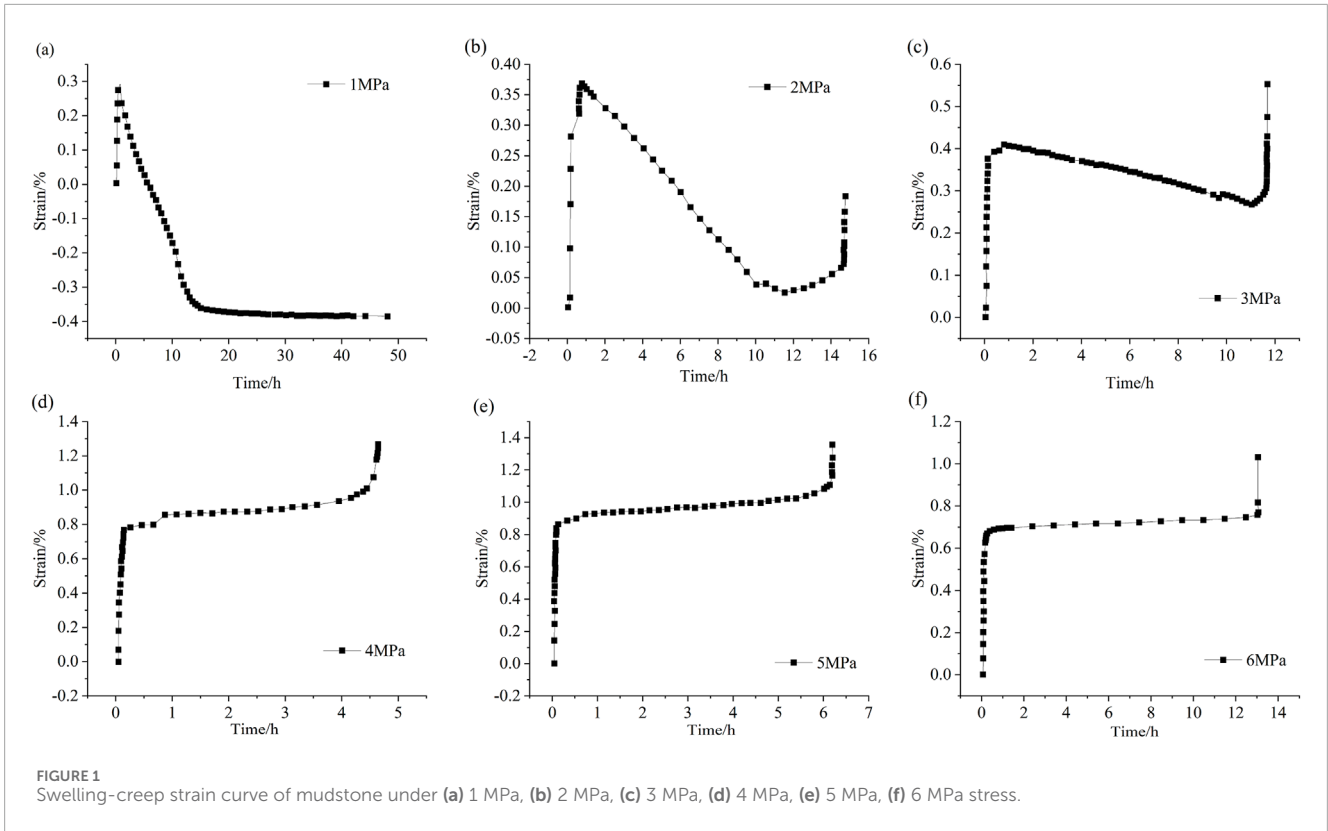
where σ is positive with tensile stress, $P(\varepsilon)$ is a function of the swelling strain determined by a swelling test. Parameter η is related to the clay mineral content, hydrophilicity and initial water content of the rock.

The value of η can be determined according to Equation 3 (Sun, 1999):

$$\eta = \frac{1}{n} \sum_{1}^{n} \frac{\Delta t}{\Delta \varepsilon} (\sigma_t + p(\varepsilon)) \qquad (3)$$

where Δt is the unit time, and $\Delta \varepsilon$ is the swelling strain increment corresponding to unit time.

Furthermore, based on the regression analysis of the swelling test (Sun, 1999), $P(\varepsilon)$ is expressed in Equation 4,.

$$\varepsilon = A \ln \frac{p_0}{p(\varepsilon)} \qquad (4)$$

where A is a non-dimensional constant, P_0 is the maximum swelling stress (MPa)

By combining Equations 2, 4, the strain equation is derived and presented in Equation 5:

$$\varepsilon = A \ln \frac{\left(p_0 + \sigma \exp\left(\frac{\varepsilon_0}{A}\right)\right) \exp\left(\frac{\sigma(t-t_0)}{A\eta_3}\right) - p_0}{\sigma} \qquad (5)$$

where t_0 is the initial time, and ε_0 is the initial strain.

3.3 Nonlinear damper

As shown in Figure 4, ND is employed to characterize the accelerated creep characteristics of the red-bed mudstone in this study.

The one-dimensional strain equation of the ND model is presented in Equation 6:

$$\sigma = \eta(n, t)\varepsilon = \eta \exp(-nt)\dot{\varepsilon} \qquad (6)$$

FIGURE 4
ND model.
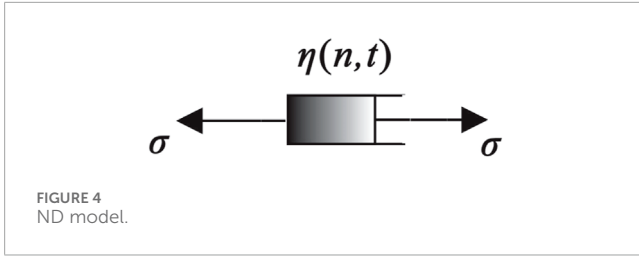
where $\eta(n,t)$ is the viscosity coefficient related to time t and parameter n.

Furthermore, the derivative is calculated and shown in Equation 7:

$$\dot{\eta}(n,t) = -n\eta \exp(-nt) \tag{7}$$

Equation 7 indicates that when $n > 0$, η decreases over time, signifying accelerated creep characteristics. Conversely, when $n < 0$, η increases with time, representing attenuated creep characteristics. When $n = 0$, η remains constant, and the ND element degenerates into a standard damper.

3.4 The swelling-creep model for red-bed mudstone

The swelling-creep model of red mudstone, as depicted in Figure 5, has been established by serially connecting the burgers model, swelling model, and ND.

In Figure 5, σ_1 and ε_1 are the stress and strain of burgers body, respectively; σ_2 and ε_2 are the stress and strain of the swelling model, respectively; σ_3 and ε_3 are the stress and strain of ND, respectively. The stress-strain equations are expressed in Equations 8–12:

$$\sigma = \sigma_1 = \sigma_2 = \sigma_3 \tag{8}$$

$$\varepsilon = \varepsilon_1 + \varepsilon_2 + \varepsilon_3 \tag{9}$$

$$\varepsilon_1 = \frac{\sigma}{E_1} + \frac{\sigma}{\eta_1}t + \frac{\sigma}{E_2}\left[1 - \exp\left(-\frac{E_2}{\eta_2}t\right)\right] \tag{10}$$

$$\varepsilon_2 = A \ln \frac{\left(p_0 + \sigma \exp\left(\frac{\varepsilon_0}{A}\right)\right)\exp\left(\frac{\sigma(t-t_0)}{A\eta_3}\right) - p_0}{\sigma} \tag{11}$$

$$\varepsilon_3 = \frac{\sigma}{n\eta_4}(\exp(nt) - 1) \tag{12}$$

Given the initial condition $t_0 = 0$, $\varepsilon_0 = 0$, according to Equations 8–12, the creep equation is derived and presented in Equation 13:

$$\varepsilon = \frac{\sigma}{E_1} + \frac{\sigma}{\eta_1}t + \frac{\sigma}{E_2}\left[1 - \exp\left(-\frac{E_2}{\eta_2}t\right)\right]$$
$$+ A \ln \frac{(p_0 + \sigma)\exp\left(\frac{\sigma t}{A\eta_3}\right) - p_0}{\sigma} + \frac{\sigma}{n\eta_4}(\exp(nt) - 1) \tag{13}$$

4 Verification of the swelling-creep model and the parameter identification

4.1 Parameter identification and model verification

There are nine parameters that need to be determined in the swelling-creep model. Parameters A and P_0 were obtained from the swelling experiment of the red-bed mudstone. Parameter E_1 can be determined by the initial strain. Parameters η_1 can be determined by the slope of the constant creep stage. The other parameters, including E_2, η_2, η_3, η_4, n, were determined by the least-square method. The identification results of model parameters are shown in Table 1.

The comparison of the fitting curve with the experimental curve is depicted in Figure 6, The application of the swelling-creep model proposed in this study adeptly captures the deformation characteristics of red mudstone across various stages.

4.2 Sensitivity analysis of parameters

As shown in Figure 7, based on the fitted strain data under a load of 2 MPa (Sample ID:2), a parametric study was conducted to investigate the effects of η_3, η_4, n on the strain. As shown in Figure 7A, the swelling deformation of the red mudstone is significantly influenced by η_3, with the strain rate inversely proportional to the value of η_3. On the other hand, the accelerated creep characteristics of the red mudstone are primarily influenced by parameters η_4 and n. As parameter n increases or parameter η_4 decreases, the mudstone enters the accelerated creep stage sooner (Figures 7B, C).

5 Implementation of the swelling-creep model in FLAC[3D]

5.1 The three-dimensional form of the model

Furthermore, to enable the swelling-creep model to characterize the plastic deformation of rocks, a plastic element, namely, the Mohr-Coulomb model (M-C), is serially connected in the model (Figure 8).

As shown in Equation 14, the total strain (ε_{ij}) of the rock consists of five components: Maxwell strain (ε^M), Kelvin strain (ε^K), swelling body strain (ε^S), ND strain (ε^{ND}), and plastic body strain (ε^P).

$$\varepsilon_{ij} = \varepsilon^M + \varepsilon^K + \varepsilon^S + \varepsilon^{ND} + \varepsilon^P \tag{14}$$

Equation 14 can be expressed in terms of the strain deviation rate, as shown in Equation 15:

$$\dot{e}_{ij} = \dot{e}^M + \dot{e}^K + \dot{e}^S + \dot{e}^{ND} + \dot{e}^P \tag{15}$$

where $\dot{e}_{ij}$, $\dot{e}_{ij}^m$, $\dot{e}_{ij}^k$, $\dot{e}_{ij}^S$, $\dot{e}_{ij}^{ND}$, $\dot{e}_{ij}^P$ represent the strain deviation rate of the total model, Maxwell body, Kelvin body, swelling body, ND, plastic body, respectively.

FIGURE 5
A new swelling-creep coupled model.
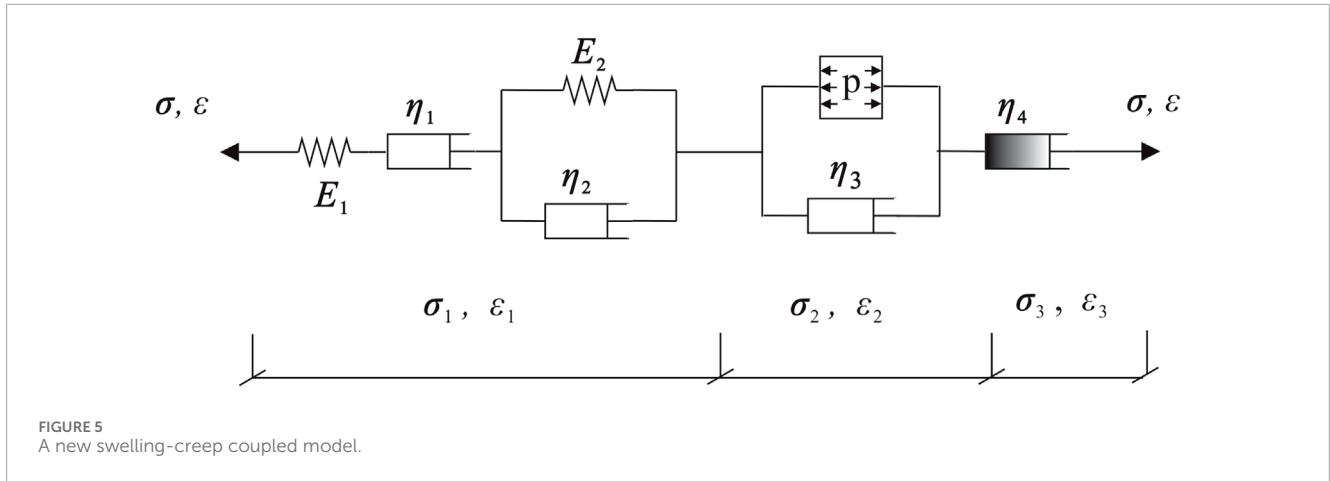
TABLE 1 Parameters identification results of swelling-creep model.

Sample ID	σ/MPa	E_1/GPa	E_2/GPa	η_1/GPa·h	η_2/GPa·h	η_3/GPa·h	η_4/GPa·h	A	P_0/MPa	n
No.1	−1	0.33	51	310	42	3.1	110	0.0036	6.5	0
No.2	−2	0.52	21	120	19	5.7	2e18	0.004	6.0	2.9
No.3	−3	0.7	46	240	35	15	1e15	0.004	6	3.1
No.4	−4	0.5	151	20	110	0.05	4.1e5	0.003	4	3.1
No.5	−5	0.6	78	20	56	0.07	6e7	0.003	4	3
No.6	−6	1.1	64	80	61	0.05	4.1e16	0.003	4	3

FIGURE 6
Comparison of the fitting curve with the experimental curve under (a) 1 MPa, (b) 2 MPa, (c) 3 MPa, (d) 4 MPa, (e) 5 MPa, (f) 6 MPa stress.

FIGURE 7
Sensitivity analysis graph or (a) η_3, (b) η_4, (c) n.

FIGURE 8
The 3D form of the swelling-creep model.

FIGURE 9
Rock sample for numerical simulation.
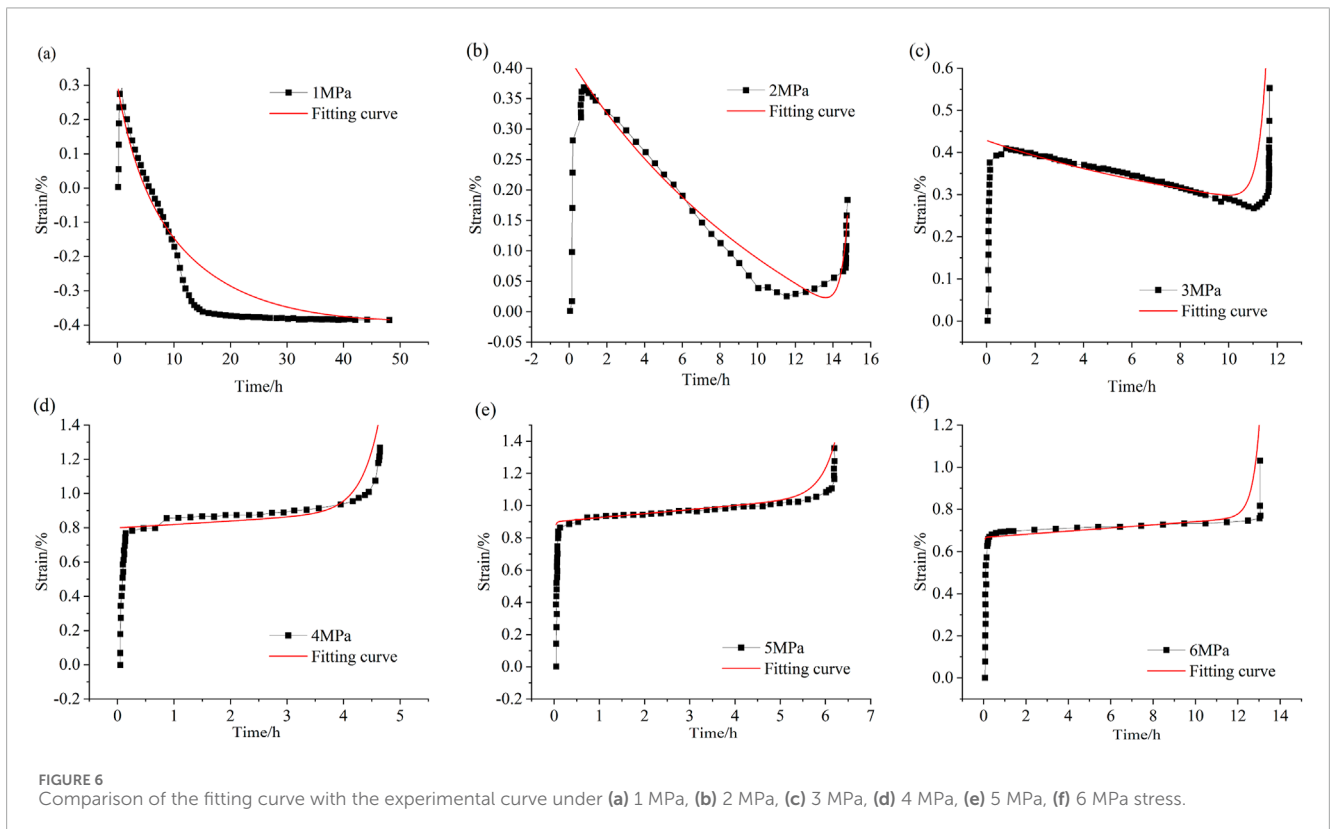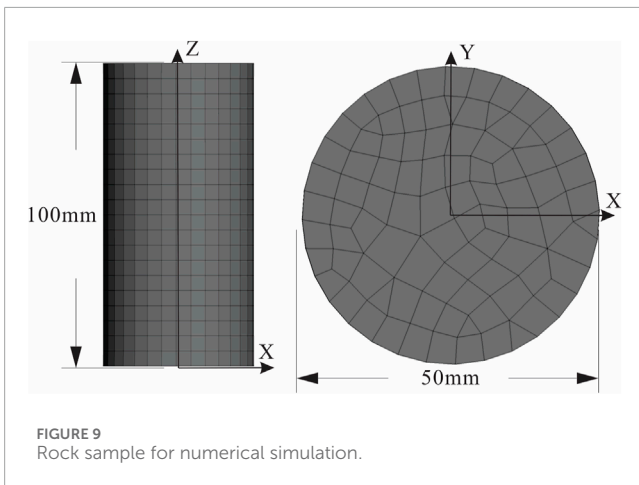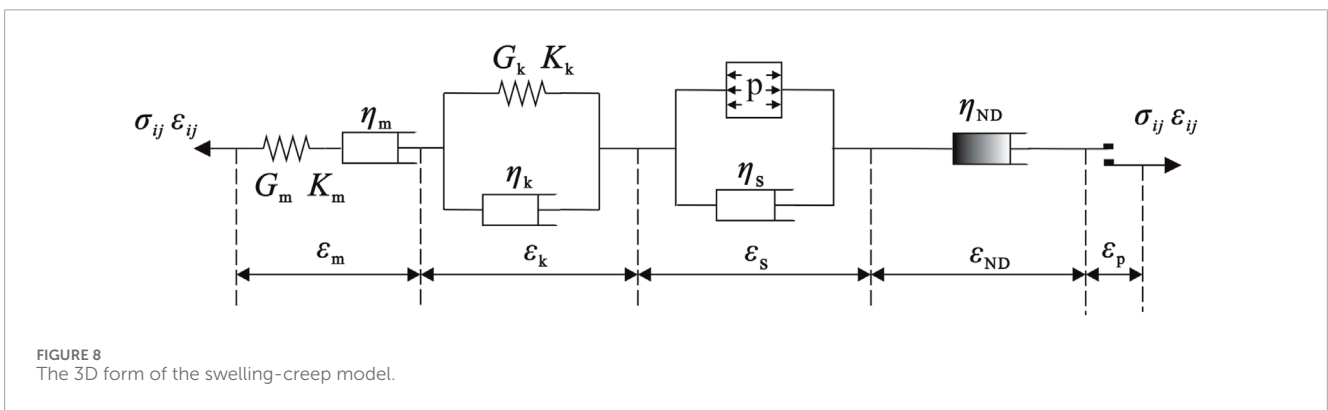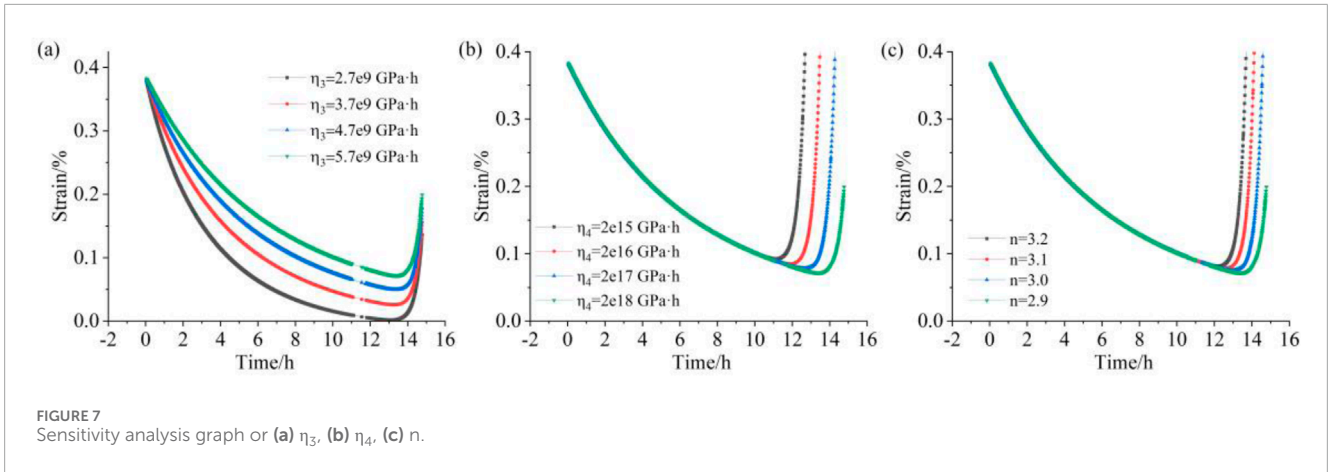
For the Maxwell element, the strain deviation rate is given by Equation 16:

$$\dot{e}_{ij}^{M} = \frac{\dot{S}_{ij}}{2G^{M}} + \frac{S_{ij}}{2\eta^{M}} \tag{16}$$

For the Kelvin element, the strain deviation rate is given by Equation 17:

$$S_{ij} = 2\eta^{K}\dot{e}_{ij}^{K} + 2G^{K}e_{ij}^{K} \tag{17}$$

For the swelling element, the strain deviation rate is given by Equation 18:

$$S_{ij} = 2\eta^{S}\dot{e}_{ij}^{S} - 2p_0 \exp\left(-\frac{e_{ij}^{S}}{A}\right) \tag{18}$$

For the ND element, the strain deviation rate is given by Equation 19:

$$S_{ij} = 2\eta(n,t)\dot{e}_{ij}^{ND} \tag{19}$$

For the plastic element, the strain deviation rate is described by Equations 20, 21:

$$\dot{e}_{ij}^{P} = \lambda \frac{\partial g}{\partial \sigma_{ij}} - \frac{1}{3}\dot{e}_{vol}^{P}\delta_{ij} \tag{20}$$

$$\dot{e}_{vol}^{P} = \lambda\left[\frac{\partial g}{\partial \sigma_{11}} + \frac{\partial g}{\partial \sigma_{22}} + \frac{\partial g}{\partial \sigma_{33}}\right] \tag{21}$$

where $\dot{e}_{vol}^{P}$, $\dot{e}_{vol}$ represents the volumetric strain rate generated by the plastic body and the total model.

The relationship between volumetric stress and volumetric strain is given by Equation 22:

$$\dot{\sigma}_0 = K\left(\dot{e}_{vol} - \dot{e}_{vol}^{P}\right) \tag{22}$$

where $\dot{\sigma}_0$ represents the volumetric strain rate.
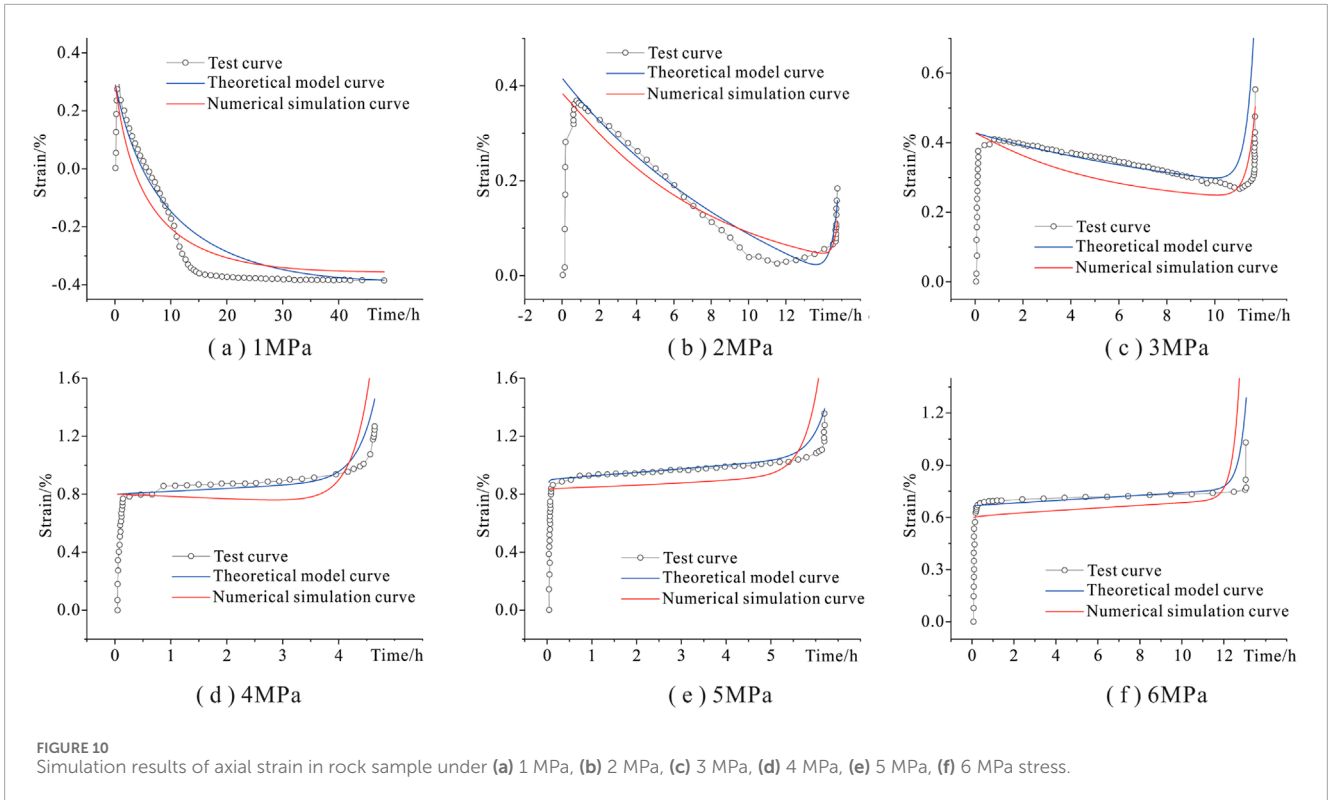
FIGURE 10
Simulation results of axial strain in rock sample under **(a)** 1 MPa, **(b)** 2 MPa, **(c)** 3 MPa, **(d)** 4 MPa, **(e)** 5 MPa, **(f)** 6 MPa stress.

TABLE 2 Numerical simulation scheme and parameter settings.

Sample ID	σ/MPa	E_1/GPa	E_2/GPa	η_1/GPa·h	η_2/GPa·h	η_3/GPa·h	η_4/GPa·h	A	P_0/MPa	n
No.7	2	0.52	21	120	19	5.7e10	2e18	0.004	6.0	2.9
No.8	2	0.52	21	120	19	5.7	2e18	0.004	6.0	2.9
No.9	4	0.52	21	120	19	5.7e10	2e18	0.004	6.0	2.9
No.10	4	0.52	21	120	19	5.7	2e18	0.004	6.0	2.9
No.11	6	0.52	21	120	19	5.7e10	2e18	0.004	6.0	2.9
No.12	6	0.52	21	120	19	5.7	2e18	0.004	6.0	2.9

5.2 The finite difference form of the swelling-creep model

The strain increment form of Equation 15 is as follows:

$$\Delta\dot{e}_{ij} = \Delta\dot{e}^{M} + \Delta\dot{e}^{K} + \Delta\dot{e}^{S} + \Delta\dot{e}^{ND} + \Delta\dot{e}^{P} \tag{23}$$

where $\Delta\dot{e}_{ij}$, $\Delta\dot{e}_{ij}^{M}$, $\Delta\dot{e}_{ij}^{K}$, $\Delta\dot{e}_{ij}^{S}$, $\Delta\dot{e}_{ij}^{ND}$, $\Delta\dot{e}_{ij}^{P}$ represent the strain deviation increment of the total model, Maxwell body, Kelvin body, swelling body, ND body, plastic body, respectively.

By applying the central difference method, Equations 16–19 are reformulated as Equations 24–27:

$$\Delta e_{ij}^{M} = \frac{\Delta S_{ij}}{2G^{M}} + \frac{\overline{S}_{ij}}{2\eta^{M}}\Delta t \tag{24}$$

$$\Delta e_{ij}^{K} = \frac{\overline{S}_{ij}}{2\eta^{K}}\Delta t - \frac{G^{K}\overline{e}_{ij}^{K}}{\eta^{K}}\Delta t \tag{25}$$

$$\Delta e_{ij}^{S} = \frac{p_0 \exp\left(-\overline{e}_{ij}^{S}/A\right)}{\eta^{S}}\Delta t + \frac{\overline{S}_{ij}}{2\eta^{S}}\Delta t \tag{26}$$

$$\Delta e_{ij}^{ND} = \frac{\overline{S}_{ij}}{2\eta^{ND}(n,t)}\Delta t \tag{27}$$

Notation convention: uppercase superscript N and O respectively denote the new and old values within a time increment step, and $\Delta e = \Delta e^{N} - \Delta e^{O}$, $\Delta S = \Delta S^{N} - \Delta S^{O}$, $\overline{S} = \Delta S^{N} + \Delta S^{O}$, $\overline{e} = \Delta e^{N} + \Delta e^{O}$.

Additionally, the plasticity rules for the plastic body are extensively explained in the FLAC^{3D} help documentation.

By substituting Equations 24–27 into Equation 23, the updated deviatoric stress is derived, as shown in Equations 28, 29:

$$S_{ij}^{N} = \frac{1}{a}\left(\Delta e_{ij} + bS_{ij}^{O} + \frac{G^{K}\overline{e}_{ij}^{K}}{\eta^{K}}\Delta t - \frac{P_0 \exp\left(-\overline{e}_{ij}^{S}/A\right)}{\eta^{S}}\Delta t - \Delta e^{P}\right) \tag{28}$$
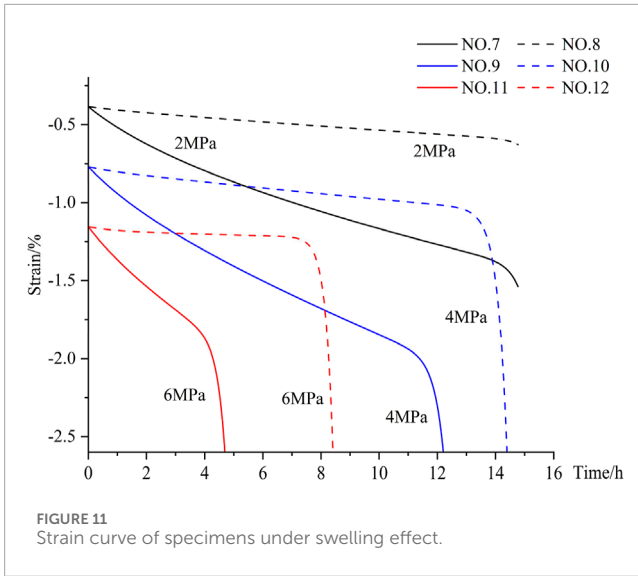
FIGURE 11
Strain curve of specimens under swelling effect.

$$\begin{pmatrix} a = \dfrac{1}{2G^{\mathrm{M}}} + \dfrac{\Delta t}{4}\left(\dfrac{1}{\eta^{\mathrm{M}}} + \dfrac{1}{\eta^{\mathrm{K}}} + \dfrac{1}{\eta^{\mathrm{S}}} + \dfrac{1}{\eta^{\mathrm{ND}}(n,t)}\right) \\[3mm] b = \dfrac{1}{2G^{\mathrm{M}}} - \dfrac{\Delta t}{4}\left(\dfrac{1}{\eta^{\mathrm{M}}} + \dfrac{1}{\eta^{\mathrm{K}}} + \dfrac{1}{\eta^{\mathrm{S}}} + \dfrac{1}{\eta^{\mathrm{ND}}(n,t)}\right) \end{pmatrix} \quad (29)$$

Furthermore, Equation 22 can be expressed as Equation 30:

$$\sigma_0^{\mathrm{N}} = \sigma_0^{\mathrm{O}} + K\left(\Delta e_{\mathrm{vol}} - \Delta e_{\mathrm{vol}}^{\mathrm{P}}\right) \quad (30)$$

In summary, the stress-strain relationship of the swelling-creep model can be represented by Equations 29, 30.

6 Application of the swelling-creep model in FLAC$^{\mathrm{3D}}$

The swelling-creep model's constitutive equations in differential form were compiled into a.dll file using the C++ language on the Visual Studio 2010 platform. Subsequently, development was carried out using the UDM interface of FLAC$^{\mathrm{3D}}$.

To validate the correctness and practicality of the developed swelling-creep model, a mudstone specimen model with the same specifications as the laboratory test was created (Figure 9). The model consists of 2,119 zones and 2,177 gridpoints.

6.1 Verification of the model's accuracy and applicability

Normal constraints were applied to the bottom surface of the model, while axial loads of −1 MPa, −2 MPa, −3 MPa, −4 MPa, −5 MPa, and −6 MPa were separately applied to the top surface of the model. Upon applying the parameter identification results from Table 1 to the model, the simulated results of axial strain are depicted in Figure 10. The results revealed that utilizing the swelling-creep model in FLAC$^{\mathrm{3D}}$ software for numerical simulations can effectively capture the swelling and creep characteristics of red-bed

mudstone. It is important to clarify that the initial stage of the test curves shown in Figure 10 represents the rapid compression phase of red-bed mudstone after the application of load. Compared to the subsequent hydration-swelling deformation, this initial phase is analogous to elastic deformation. Since the focus of this study is to develop a model that describes the coupled hydration-swelling deformation characteristics of red-bed mudstone, the simulation curve does not fully match the initial deformation phase.

6.2 Numerical simulation of swelling-creep deformation in red-bed mudstone under tensile stress

Although researchers have conducted coupled swelling-creep tests on the red-bed mudstone, they have not considered the situation where the direction of creep is consistent with the direction of swelling. Based on this issue, this study will simulate the deformation process of red-bed mudstone samples under the combined action of tensile and swelling stresses using the swelling-creep model on the FLAC$^{\mathrm{3D}}$ platform.

The numerical model remains unchanged (Figure 9), and the numerical simulation scheme is presented in Table 2. It should be noted that, setting the parameter η_3 of the samples (NO.7, NO.9, NO.11) to 5.7e10 is intended to mitigate the influence of swelling deformation on rock deformation. These parameter settings enable a comparative analysis between NO.7, NO.9, NO.11, and NO.8, NO.10, NO.12, respectively.

As shown in Figure 11, water absorption and swelling in the red mudstone significantly accelerate the strain rate, reducing the time required to enter the accelerated creep stage. Moreover, the axial load plays a crucial role in the deformation process. When the load increases from 2 MPa to 4 MPa and 6 MPa, the stable creep rate of the specimen rises from 0.0006/h to 0.0009/h and 0.0025/h, respectively.

7 Conclusion

A swelling-creep model was established to depict attenuated creep, swelling deformation, and accelerated creep of red-bed mudstone. This model was subsequently implemented in FLAC$^{\mathrm{3D}}$, and the swelling-creep deformation under tensile stress in red-bed mudstone was analyzed through simulation. The conclusions are summarized as follows.

(1) By fitting and comparing with experimental data, it has been validated that the proposed swelling-creep model in this study can effectively describe the various stages of swelling and creep characteristics of red-bed mudstone.

(2) The three-dimensional constitutive equations of swelling-creep were derived, followed by secondary development in FLAC$^{\mathrm{3D}}$. Standard mudstone specimens were then subjected to uniaxial compression simulation, and the simulation results were found to be consistent with experimental data, indicating the applicability of the developed model.

(3) When red-bed mudstone is subjected to axial tensile stress, the swelling effect markedly enhances the axial strain rate, expediting the transition to the accelerated creep stage. As the

load increases from 2 MPa to 4 MPa and 6 MPa, the stable creep rate of the specimen increases from 0.0006/h to 0.0009/h and 0.0025/h, respectively.

Data availability statement

The raw data supporting the conclusions of this article will be made available by the authors, without undue reservation.

Author contributions

HY: Writing - original draft, Writing–review and editing. FY: Conceptualization, Data curation, Investigation, Methodology, Software, Supervision, Writing–review and editing. CZ: Formal Analysis, Project administration, Validation, Writing–review and editing. JY: Investigation, Project administration, Software, Writing–review and editing. QW: Conceptualization, Formal Analysis, Writing–review and editing. JW: Formal Analysis, Software, Writing–review and editing.

Funding

Conflict of interest

The authors declare that the research was conducted in the absence of any commercial or financial relationships that could be construed as a potential conflict of interest.

Generative AI statement

The author(s) declare that no Generative AI was used in the creation of this manuscript.

Publisher's note

References

Chen, K., Liu, X., Yuan, S., Ma, J., Chen, Y., and Jiang, G. (2025). Effect of stress state and stress path on small strain properties of red mudstone fill material. *Bull. Eng. Geol. Environ.* 84 (1), 35–18. doi:10.1007/s10064-024-04058-1

Chen, K., Yuan, S., Pan, S., Ma, J., and Liu, X. (2023). Energy-based insight into characterization of shakedown behavior of fully weathered red mudstone. *Soils Found.* 63 (5), 101360. doi:10.1016/j.sandf.2023.101360

Chen, K., Zhang, R., Liu, X., Wang, H., and Cai, H. (2024). Investigation on long-term dynamic properties of decomposed mudstone as a substitutive fill material in railway subgrade. *Constr. Build. Mater.* 449, 138384. doi:10.1016/j.conbuildmat.2024.138384

Doostmohammadi, R., Moosavi, M., Mutschler, T., and Osan, C. (2009). Influence of cyclic wetting and drying on swelling behavior of mudstone in south west of Iran. *Environ. Geol.* 58, 999–1009. doi:10.1007/s00254-008-1579-3

Einstein, H. H. (1989). Suggested methods for laboratory testing of argillaceous swelling rocks. *Intl J Rock Mech & Min. Sci & Geomechanic Abs* 26 (5).

Fan, Q., and Gao, Y. (2007). Study on creep properties and nonlinear creep model of soft rock. *Yanshilixue Yu Gongcheng Xuebao/Chinese J. Rock Mech. Eng.* 26 (2), 391–396.

Hashiba, K., and Fukui, K. (2016). Time-dependent behaviors of granite: loading-rate dependence, creep, and relaxation. *Rock Mech. Rock Eng.* 49, 2569–2580. doi:10.1007/s00603-016-0952-x

Hayano, K., Matsumoto, M., Tatsuoka, F., and Koseki, J. (2001). Evaluation of time-dependent deformation properties of sedimentary soft rock and their constitutive modeling. *Soils Found.* 41 (2), 21–38. doi:10.3208/sandf.41.2_21

Huang, K., Dai, Z., Yan, C., and Chen, S. (2023a). Numerical study on the swelling and failure of red-layer mudstone subgrade caused by humidity diffusion. *Comput. Geotechnics* 156, 105272. doi:10.1016/j.compgeo.2023.105272

Huang, K., Dai, Z., Yan, C., Yu, F., Zhang, W., and Chen, S. (2024). Swelling behaviors of heterogeneous red-bed mudstone subjected to different vertical stresses. *J. Rock Mech. Geotechnical Eng.* 16 (5), 1847–1863. doi:10.1016/j.jrmge.2023.08.004

Huang, K., Yu, F., Zhang, W., Tong, K., Li, S., Guo, J., et al. (2023b). Experimental and numerical simulation study on the influence of gaseous water on the mechanical properties of red-layer mudstone in central Sichuan. *Rock Mech. Rock Eng.* 56 (4), 3159–3178. doi:10.1007/s00603-023-03228-z

Jia, J., Yu, F., Tan, Y., and Gao, X. (2021). Experimental investigations on rheological properties of mudstone in kilometer-deep mine. *Adv. Civ. Eng.* 2021 (1), 6615379. doi:10.1155/2021/6615379

Kong, L. W., Zeng, Z. X., Bai, W., and Wang, M. (2018). Engineering geological properties of weathered swelling mudstones and their effects on the landslides occurrence in the Yanji section of the Jilin-Hunchun high-speed railway. *Bull. Eng. Geol. Environ.* 77, 1491–1503. doi:10.1007/s10064-017-1096-2

Liu, X. F., Chen, K., Yuan, S. Y., Ma, J., Chen, Y. H., and Jiang, G. L. (2024). Experimental study on the small strain stiffness-strength of a fully weathered red mudstone. *Constr. Build. Mater.* 438, 137058. doi:10.1016/j.conbuildmat.2024.137058

Lu, Y., Wang, L., Sun, X., and Wang, J. (2017). Experimental study of the influence of water and temperature on the mechanical behavior of mudstone and sandstone. *Bull. Eng. Geol. Environ.* 76, 645–660. doi:10.1007/s10064-016-0851-0

Madsen, F. T. (1999). International society for rock mechanics commission on swelling rocks and commission on testing methods: suggested methods for laboratory testing of swelling rocks. *Int. J. Rock Mech. Min. Sci.* 36, 291–306.

Steiner, W. (1993). "Swelling rock in tunnels: rock characterization, effect of horizontal stresses and construction procedures,"*Int. J. rock Mech. Min. Sci. & geomechanics Abstr.* 30. 361–380. doi:10.1016/0148-9062(93)91720-4

Sun, J. (1999). *Rheology of geotechnical materials and its application in engineering.* Beijing, China: China Architecture and Building Press.

Yu, H. C., Liu, H. D., Huang, Z. Q., and Shi, G. C. (2017). Experimental study on time-dependent behavior of silty mudstone from the Three Gorges Reservoir Area, China. *KSCE J. Civ. Eng.* 21, 715–724. doi:10.1007/s12205-016-3645-9

Zhang, C. L., Wieczorek, K., and Xie, M. L. (2010). Swelling experiments on mudstones. *J. Rock Mech. Geotechnical Eng.* 2 (1), 44–51.

Zhang, X., Li, Y., Zhang, S., and Huo, B. R. (2004). Creep theory of soft rock and its engineering application. *Chin. J. rock Mech. Eng.* 23 (10), 1635–1639.

Zhang, Z. (2020). Study on the characteristics of swelling-creep and damage of soft rock under hydration: hunan universityof science and Technology, phd thesis.

Zhong, Z. B., Li, A. H., Deng, R. G., Wu, P. P., and Xu, J. (2019). Experimental study on the time-dependent swelling characteristics of red-bed mudstone in Central Sichuan. *Chin. J. Rock Mech. Eng.* 38 (1), 76–86.